Development of a 3-D Dynamic Fracture Process Analysis code to Simulate Intermediate Loading Rate

Development of a 3-D Dynamic Fracture Process Analysis code to Simulate Intermediate Loading Rate

D. Fukuda[1], S.H. Cho[2], G.J. Min[2], H.Y. LIU[3], K. Kodama[1], F. Fujii[1]

[1]Faculty of Engineering, Hokkaido University, Hokkaido 060-8628, Japan
[2]Department of Mineral Resources and Energy Engineering, Jeonbuk National University, Jeollabuk-do, 561-756, South Korea
[3]School of Engineering, College of Sciences and Engineering, University of Tasmania, Hobart, Tasmania 7001, Australia

The corresponding author's e-mail address: d-fukuda@frontier.hokudai.ac.jp

Abstract. For the stimulation solutions for oil and gas wells, the creation of multiple fractures that extend deep into surrounding rock formation is important to improve productivity or injectivity. For this purpose, the application of "not too slow but not too fast dynamic loading rate (hereafter intermediate dynamic loading rate)" has been proposed in the literature, which utilizes solid propellants. While previous researchers have experimentally demonstrated their applicability, our understanding of the detailed mechanism of rock fracturing for such an intermediate dynamic loading rate has not been mature enough. We have self-developed a state-of-the-art 3D combined finite-discrete element simulator that can model the complex dynamic fracture process of rocks. This paper applied the developed code to investigate its applicability to this class of problem characterized by the intermediate dynamic loading rate. NRC (new rock cracker) based on the water vaporized pressure due to the thermit reaction of the non-explosive ingredients was used. Based on the measured pressure as an input to the developed code, the 3D dynamic fracture process analysis (DFPA) was conducted. The involving dynamic fracture process and resultant fracture pattern were discussed. In addition, the required future tasks for more reasonable numerical simulation were also pointed out.

1. Introduction

For the stimulation solutions for oil and gas wells, creating multiple fracture planes (i.e., more than two macroscopic fracture planes) extending deep into surrounding rock formations is very important to improve productivity or injectivity. However, conventional hydraulic fracturing cannot achieve this goal because of the "too slow" loading rate. On the other extreme, when the detonation of high explosive is applied, the crushing zone characterized by too many short radial cracks around the wellbore tends to be generated, which may deteriorate the productivity or injectivity when the in-situ stress level is very high. As an alternative, the application of "not too slow but not too fast dynamic loading rate (hereafter intermediate dynamic loading rate)" has been proposed, which utilizes solid propellants. Their applicability has been experimentally demonstrated by previous researchers (e.g., [1][2]).

However, our understanding of the detailed mechanism of rock fracturing for such an intermediate dynamic loading rate has not been mature enough. The reason is that the involving processes include: (i)gas expansion whose pressure acts on the charge hole surface, (ii)3-dimensionally complex and

rapid dynamic fracture process of rock, and (iii)solid-gas interaction in the newly generated fractures. This results in the necessity of a high-fidelity three-dimensional (3D) numerical fracture process simulator. We have self-developed a state-of-the-art 3D numerical simulator based on the combined finite-discrete element method (FDEM). The code can model the stress wave propagation of intact rock, the transition from continuum to discontinuum (i.e., initiation, propagation, and coalescence of microcracks resulting in the formation of macro cracks), and very complex surface contact interaction between newly generated macroscopic fracture surfaces ([3],[4]). In [3] and [4], the applicability of the code was demonstrated against the dynamic Brazilian test and dynamic uniaxial compression test of marble specimens, which indicates the applicability of the code to the intermediate dynamic loading.

In this contribution, as a first step, we conducted a fundamental investigation for the generation of multiple fractures around a charge hole using the intermediate dynamic loading rate. Since getting access to solid propellants is not easy, we alternatively utilized NRC (new rock cracker) to realize such a loading rate range. We first measured the generated pressure using NRC to show the loading characteristics of NRC. A dynamic rock breakage test using the NRC was also conducted. We numerically simulated the 3D dynamic fracture process in the dynamic rock breakage test based on the measured pressure. We also summarized the required future tasks for a better understanding of the target problem.

2. Pressure measurement of NRC

NRC utilizes the water vaporized pressure due to the thermit reaction of the non-explosive ingredients, which has been used to investigate the mechanical behavior of rocks under dynamic loading at intermediate dynamic loading rate (approximate strain rate range = 10^{-1} ~10^{0} [1/sec]). For example, Wicaksana and Jeon [5] conducted a series of laboratory tests to obtain the uniaxial compressive strength of rocks using NRC. It was found that the strength of the tested granite and sandstone specimens increased at the range of the intermediate dynamic loading rate. They showed that the loading rate dependency of the rock strength was not consistent within such a range of the loading rate. For NRC used in this paper, the bulk density was 1250~1350(kg/m^3), the reaction temperature was 2502 K, the amount of heat generation was 409 kcal/kg, the amount of gas generation was 351 L/kg, and the specific energy was 3324 L/kg (See [6] for further detail).

To measure the pressure induced by the initiation of NRC, we prepared an experimental system, as shown in Figure 1. An acrylic block was prepared in which a charge hole and another hole (hereafter, pressure hole) connecting the near-bottom part of the charge hole and surface of the block were manufactured. An adapter for the pressure sensor was also prepared, and a Teflon tape was used for preventing gas leak between the hole surface and the adapter. A screw tap was also manufactured in the block to fix the adapter to it. Based on this, the pressure sensor (Model CY-YD-214, Sinocera) was set on the mouth of the pressure hole. To record the measured pressure signal, the pressure sensor was connected to the data acquisition system, consisting of an oscilloscope and a signal amplifier. The 10-gram NRC was charged from the bottom of the charge hole, and the initiator was set on the top of the NRC. It is worth mentioning that, although the initiator was able to initiate the NRC, the initiator itself could not cause any noticeable damage to the acrylic block. The sand stemming was applied to the collar of the charge hole, which covered the charged NRC. After installing the pressure sensor and checking the electric circuit of the data acquisition system, the acrylic block was set inside a metal chamber to ensure safety. The lid of the chamber was closed tightly during the pressure measurement.

Figures 2(a) and 2(b) show the measured pressure profile in the acrylic block and the fracture pattern after the measurement, respectively. The measured pressure profile in Figure 2(a) indicates that the rise time, i.e., the time for the pressure to achieve peak value, was of the order of 100 ~ 150 μs, and the pressure gradually decayed after the peak. Figure 2(b) indicates that the block was split into two pieces, and multiple fractures were not observed around the charge hole. Due to the existence of the pressure hole, the formation of a cone-shaped fragment was also observed.

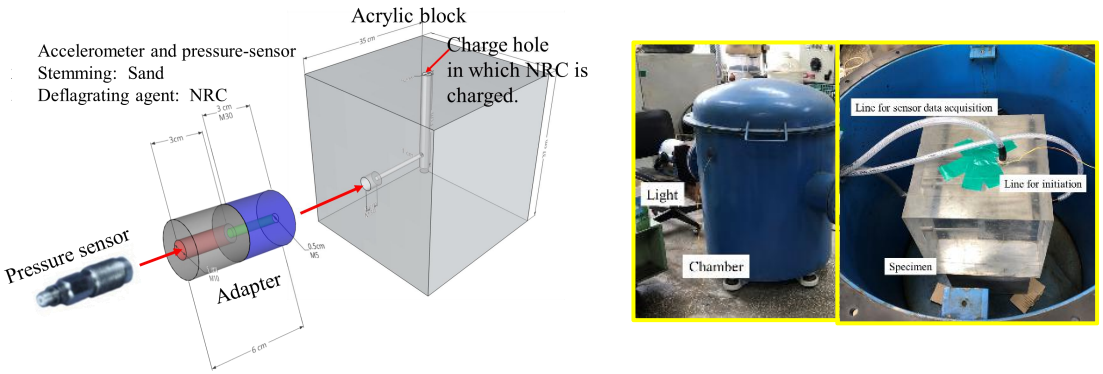

Figure 1 Experimental system to measure pressure in the charge hole due to the initiation of NRC.

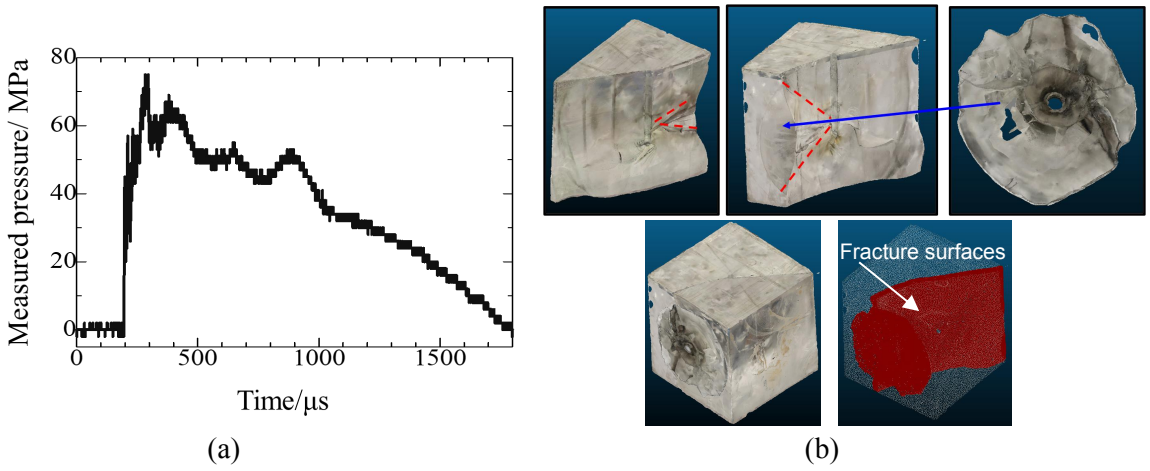

Figure 2 (a)Measured pressure profile and (b)fracture pattern of the acrylic block after the measurement.

3. Rock breakage test using NRC

To understand the typical fracture pattern of rocks due to the intermediate dynamic loading by NRC, a breakage test of a cubic rock block was conducted using 50-gram NRC. A gneiss rock block having the dimension shown in Figure. 3(a) was prepared. The picture of the actual gneiss block is shown in Figure. 3(b). The Φ20 mm charge hole with 400 mm length was drilled in the rock block, and the NRC initiator (200 mm length) was set just above the hole bottom. Then, the sand stemming was applied. The commencement of the initiation started from the top of the initiator toward the hole bottom. For safety reasons, the charged rock block was covered by the nonwoven cloth, explosion-proof sheet, and rubber-mat to avoid the flying rock due to fragmentation, and thus we could not observe the fracture process. The breakage test was conducted at Jeonbuk national university in Korea. Physical/mechanical properties of the gneiss were investigated by Min et al. [7]. Table 1 summarizes these properties assuming the isotropic behavior.

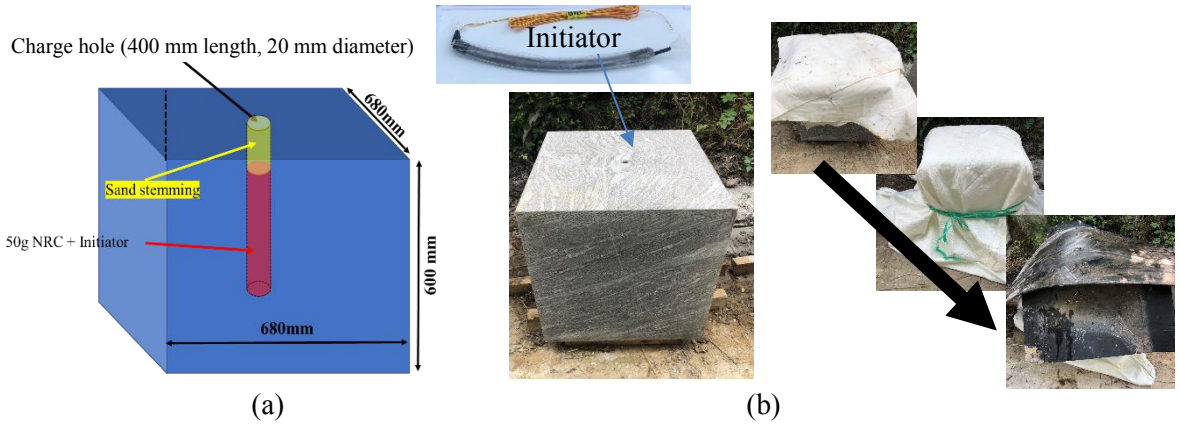

Figure 3 (a)Schematic illustration and (b) photo of gneiss block subjected to dynamic breakage test using 50-gram NRC.

The result of the breakage test is shown in Figure. 4. The fracture pattern was found to be splitting mode in which the rock block was split into two halves. The gneiss block also exhibited a similar fracture pattern to that for the acrylic block, i.e., multiple fractures were not obtained.

Table 1 Physical/mechanical properties of the gneiss [6].

V_p (m/s)	5168
V_S(m/s)	3233
Density(kg/m^3)	2700
Static BTS (MPa)	10.8
Static UCS (MPa)	152.2
Young's modulus(GPa)	68.5
Poisson's ratio	0.18
Static cohesion(MPa)	25.65
Static internal friction angle (Deg)	53.1

Note: BTS: Brazilian indirect tensile strength
UCS: Uniaxial compressive strength

Figure 4 Resultant fracture pattern after the breakage test of the gneiss block.

4. Dynamic fracture process analysis by 3D FDEM simulator

Based on the above results of the pressure measurement and the rock breakage test, a 3D FDEM rock model was prepared, and a dynamic fracture process analysis (DFPA) was conducted. Here, we briefly introduce the following three-pillar modeling concepts (i)~(iii) in the FDEM (refer to [3] and [4] for further detail of the applied FDEM code, which has incorporated parallel computation by utilizing general-purpose graphic processing units (GPGPUs)):

−(i) Modelling the continuum deformation/intact stress wave propagation using continuum solid elements (3-D tetrahedral elements).

−(ii) Modelling the transition from continuum to discontinuum, i.e., initiation and propagation of microcracks resulting in the formation of macro fracture surfaces, based on the cohesive zone model (CZM) (tensile/shear softening) using initially zero-thickness cohesive elements.
−(iii) Modelling the discontinuum behavior, i.e., complex surface contact interactions between material surfaces, including newly created macro fracture surfaces using potential-based contact mechanics.
It is clear from these pillar modeling concepts that the 3D FDEM was expected as a good candidate for the target problem.

Figure 5 shows the 3D DFPA model for the gneiss block whose dimension was the same as that in Figure 3. The input parameters for the DFPA were set based on Table1. Lame's constants were estimated from the V_p, V_s, and density in Table 1. Considering our preliminary study, including [6] using the split Hopkinson pressure bar (SHPB)-based dynamic tests for the gneiss, the dynamic strength increase factor (DIF) against static strength was identified as 1.2 for tensile strength while 1.1~1.4 for compressive strength, i.e., very small DIF. Thus, the strength increase due to the loading rate effect was not considered, and the tensile strength and the cohesion reported in Table 1 were assumed. Then, to compute mode I and II fracture energies [3], we assumed the critical crack opening and sliding displacements of the cohesive cracks to be 50 μm because of the lack of experimental data. We did not explicitly consider the stemming effect and simply applied the NRC-induced pressure to the surface of the charge hole in which NRC was placed (hereafter, NRC region). The pressure $P(t)$ in the NRC region was modeled using the following equation:

$$P(t) = \begin{cases} 0 \quad \text{for } 0 \le t \le t_s \\ P_0 \dfrac{t - t_s}{t_0} \quad \text{for } t_s \le t \le t_s + t_0 \\ P_0 e^{-\alpha\{t-(t_s+t_0)\}} \quad \text{for } t_s + t_0 \le t \end{cases} \tag{1}$$

where maximum pressure P_0 = 125 MPa, pressure rise time t_0 =150 μs, and pressure decay rate α = 2500 were assumed considering our previous experience and the above pressure measurement in Figure 2(a). Note that P_0 of 50- gram NRC used in this test was not evident instead of 10-gram in Figure 2(a), and the strength of the acryl was significantly different from that of the gneiss. The t_s ($=\|\boldsymbol{x}-\boldsymbol{x}_{init}\|/V_{deflag}$) in Eq. (1) indicates the time when the deflagration wave arrived at the point of interest, $\boldsymbol{x}$, in the NRC region. The $\boldsymbol{x}_{init}$ indicates the point in which deflagration commenced by the initiator, i.e., top of the NRC region. The deflagration wave propagation speed V_{deflag} = 1.2 km/s in the

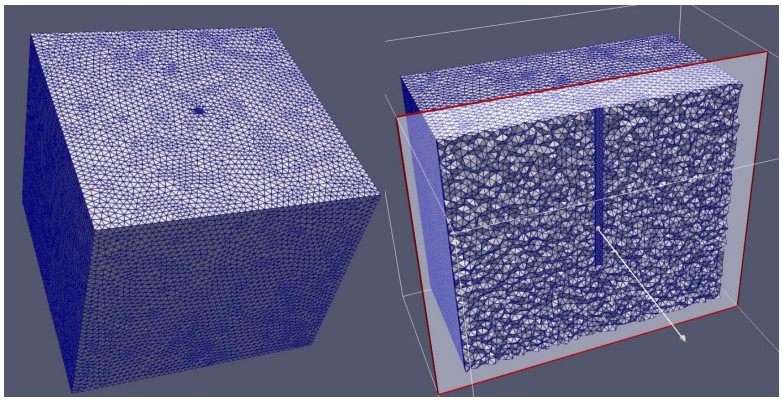

The number of nodes:
2,850,656
The number of tetrahedral elements:
712,664
The number of cohesive elements:
1,413,216

Figure 5 3D FDEM mesh used to simulate the rock breakage test of gneiss block by NRC (50g).

charge hole was assumed based on our experience. At time $t = 0$, the pressure $P(t)$ started to act from the top of the NRC region and propagated toward the hole bottom with the propagation speed of V_{deflag}. The current FDEM code has not implemented the solvers to simulate the gas dynamics and solid-gas interaction. Thus, this work assumed a simple gas zone model. In this model, we assumed a gas zone expanding from each point on the surface of the charge hole to the outer free faces with the constant nominal gas flow rate. Considering our experiences, the nominal gas flow rate was assumed to be 400 m/s. In addition, the macro fracture network (MFN) directly connected to the charge hole was computed during the simulation. Then, the NRC-induced pressure was also applied to the surfaces of the MFN included in the gas zone. For a broken cohesive element in the MFN, the value of pressure acting on that location was linearly decayed according to the distance from the charge hole surface to the position of the macro fracture, where the pressure values at the charge hole and outer free faces become $P(t)$ and 0, respectively.

Figure 6 shows the DFPA results at selected time intervals after the initiation of NRC. The left column in the figure corresponds to fracture propagation (Damage = 0(Intact) ~ 1(Macroscopic fracture)). The middle and right columns in the figure are the distributions of maximum principal stress (i.e., the most tensile side) against the clipped planes passing through the center of the model. The positive and negative values of the principal stress correspond to tension and compression, respectively. The white boxes in the figure indicate the outlines of the 3D model. At time $t = 0$, the deflagration-induced pressure started to act on the charge hole wall, and this pressure wave propagated from the top of the NRC region to the bottom of the charger hole. At time $t = 90$ μs, the deflagration had propagated for the distance of $V_{\text{deflag}} \times 90$ μs in the NRC region. It is also found that, at each height of the charge hole, the circumferential tensile stress started to horizontally propagate from the charge hole wall toward the lateral outer surfaces of the model. The circumferential tensile stress was developed immediately after applying pressure to the charge hole wall because the applied loading rate was much slower than the detonation-induced pressure. A similar tendency was also reported in the case of deflagration of nitromethane [8], in which similar loading characteristics were observed, i.e., $t_0 \approx 140$ μs. Due to this circumferential tensile stress, tensile cracks were initiated from the sidewall of the charge hole. These tensile cracks then grew into the two macroscopic fracture planes propagating toward the lateral outer boundaries of the model. During this event, the pressure acting on the surface of MFN directly connected to the charge hole extended the two macro fractures further and finally split the rock block into two halves.

The resultant fracture pattern obtained from the DFPA is shown in Figure 7 (Left). The fracture surface was relatively smooth and almost flat, which reasonably captured the fracture characteristics in the aforementioned dynamic breakage test of the gneiss block in Figure. 4. To show the effect of the pressure acting on the surface of MNF directly connected to the charge hole, another DFPA simulation was conducted using the same input parameters without applying the NRC-induced gas pressure applied on the MFN surfaces. The resultant fracture pattern is shown in Figure 7 (Right). Compared with the case with the gas zone expansion model, the fractured zone in Figure 7 (Right) was highly limited without the gas zone expansion model. Therefore, only considering stress wave due to the pressure acting on the initial charge hole wall was insufficient to split the rock block. It is worth noting that both increasing the value of P_0 or assuming much weaker rock strengths (including applying heterogeneous strength distribution) can extend the macroscopic fractures propagating from the initial charge hole wall. However, in such cases, initiation of fractures from the outer free faces (see the formation of the cross-shaped fracture on the lateral free surfaces as shown in Figures 3(a) and 4(a) in [9]) were deemed to occur although the corresponding results are omitted due to the page limitation. However, no such fractures were observed from the fracture pattern in Figure. 4. Although the deflagration of nitromethane [8] and thermit reaction (Figure 2(a)) showed very similar loading characteristics, at least in the measured pressure profile, the difference in the resultant fracture pattern is very intriguing. Thus further study would help our understanding of the target problem.

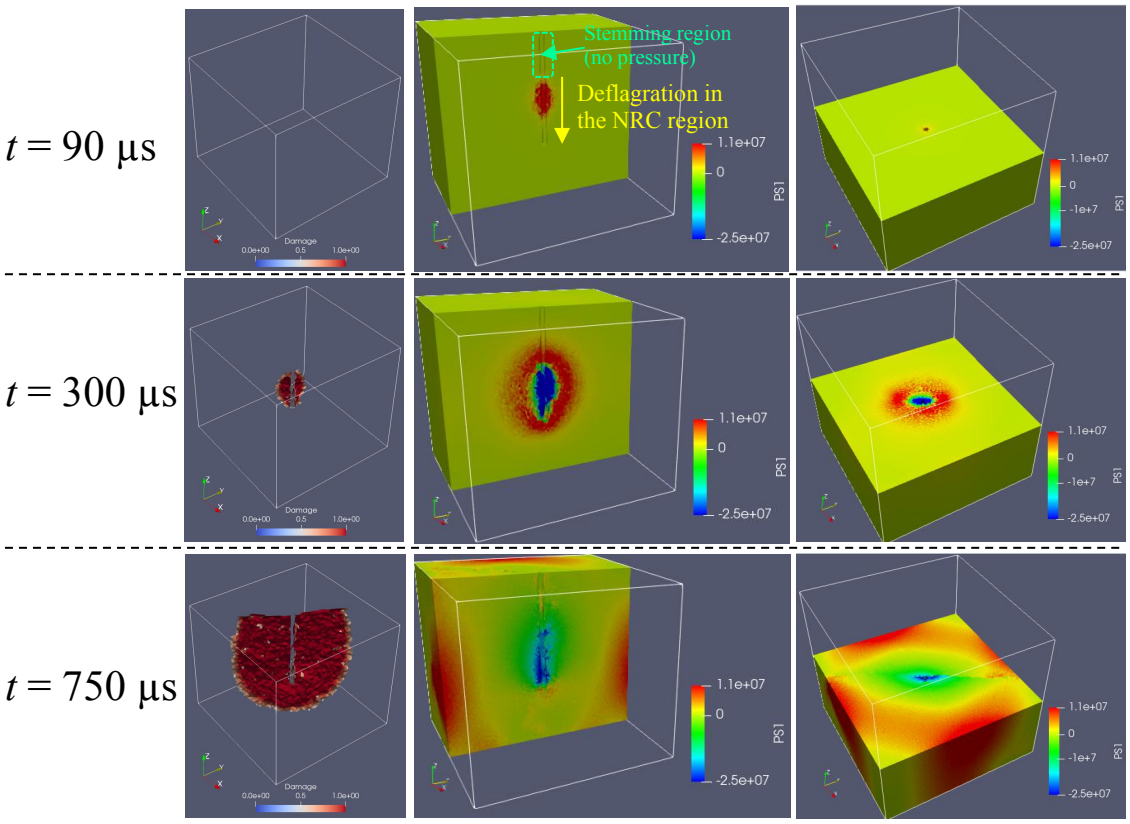

Figure 6 3D dynamic fracture process and stress wave propagation simulated by 3D FDEM.

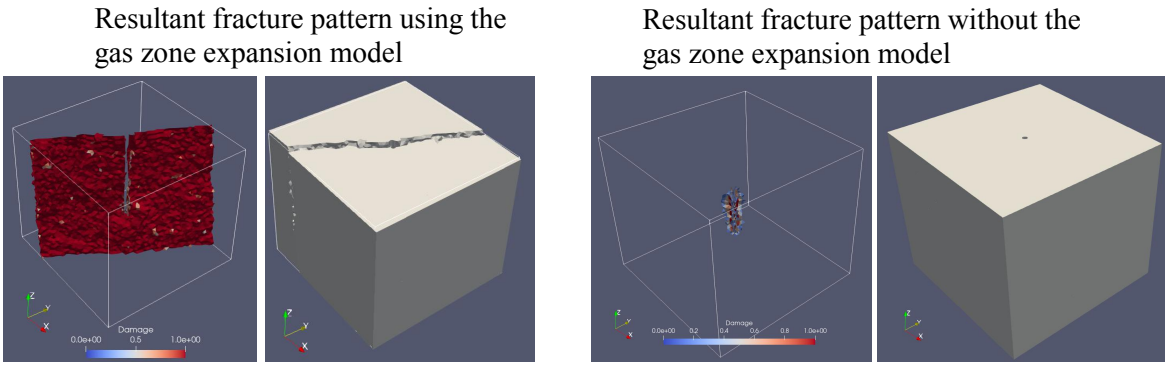

Figure 7 Comparison between the cases with/without the gas zone expansion model applying the pressure on the surfaces of MFN.

5. Conclusion and future task

This paper conducted a fundamental investigation aiming to generate multiple fractures around a charge hole using the intermediate dynamic loading rate. To realize such loading rate, NRC was utilized. The measured pressure against the initiation of 10-gram NRC in the charge hole of the acrylic block showed that the pressure rise time was of the order of 100 μs. In contrast, the resultant fracture pattern showed splitting mode in which the block was split into two halves, i.e., no multiple fractures. We also conducted the dynamic rock breakage test of the gneiss block using 50-gram NRC. The test also showed that the resultant fracture pattern was splitting mode, i.e., the rock block was split into

two halves without showing multiple fractures. Based on the measured pressure profile (rise time ~ 150 μs), the 3D DFPA, which also incorporated the simple gas zone expansion model, was conducted to model the dynamic rock breakage test of the gneiss block. The 3D DFPA simulation elucidated the detailed dynamic fracture process and also resulted in the splitting fracture mode. It was also indicated that without the gas zone expansion model, i.e., consideration of gas pressurization on the surfaces of the newly generated broken fracture network, the fracture pattern observed in the dynamic breakage test of the gneiss could not be simulated well. Therefore, we may conclude that the 3D DFPA based on the FDEM is a valuable tool to identify the detailed fracture mechanism of this class of problems. However, since our discussion in this paper was for the single breakage test against the gneiss block, more tests must be conducted to understand the detailed mechanism of the dynamic fracture due to the intermediate dynamic loading rate. Observation of dynamic fracture process using high-speed imaging and evaluation of the strain field based on the digital image correlation (DIC) is expected to be helpful. We plan to conduct similar tests using other blocks such as mortar and granite. In addition, the gas zone expansion model applied in this study was extremely simple, and detailed modeling of deflagration and compressible gas flow into the newly generated fracture network must be considered on which the authors are currently working. Therefore, by implementing/modeling the reasonable computational gas dynamics solver and the solid-gas interaction during the dynamic fracture process, the quality of the 3D numerical simulation must be improved further. Then, the possibility and optimum loading condition for generating the multiple fractures around the charge hole will be identified in our future study.

Acknowledgements
This work was supported by JSPS KAKENHI, subject nos. 18K14165. The support is gratefully acknowledged.

References
[1] Schmidt, Richard A., et al. Multi-frac test series. Final report. No. SAND-81-1239. Sandia National Labs., Albuquerque, NM (USA), 1981.
[2] R.A. Schmidt, W.M. Ashley, Solid propellants provide cost-effective stimulation in marginal wells, World Oil, Petroleum Technology Supplement, World Oil, 2001.
[3] D. Fukuda, M. Mohammadnejad, H.Y. Liu, Q.B. Zhang, J. Zhao, S. Dehkhoda, A. Chan, J. Kodama and Y. Fujii, Development of a 3D Hybrid Finite-Discrete Element Simulator based on GPGPU- Parallelized Computation for Modelling Rock Fracturing Under Quasi-Static and Dynamic Loading Conditions, *RMRE*, 53:1079–1112, 2020.
[4] D. Fukuda, H. Liu, Q.B. Zhang, J. Zhao, J. Kodama, Y. Fujii, A. Chan, Modelling of dynamic rock fracture process using the finite-discrete element method with a novel and efficient contact activation scheme, *IJRMMS*, 138:doi: 10.1016/j.ijrmms.2021.104645, 2021.
[5] Y. Wicaksana, S. Jeon, Mechanical behaviour of rock subjected to uniaxial compression at intermediate strain rate, *Geosys. Eng.*, 23(5):243-250, 2020.
[6] S. Oh, S. Park, G. Min, H. Park, Y. Yoo, S. Cho, Deflagration characteristics of thermite reaction mixtures under decoupled charges, *Sci. Technol. Energetic Mater.*, 81:114-20, 2020
[7] G. Min, S. Oh, S. Park, S. Cho, Y. You, L. Park, Evaluation of the dynamic shear strength of rocks under confining pressure, 2019 *Rock Dynamics Summit*, CRC Press(1st Ed.):124-128, 2019.
[8] D. Fukuda, K. Moriya, K. Kaneko, K. Sasaki, R. Sakamoto, K. Hidani, Numerical simulation of the fracture process in concrete resulting from deflagration phenomena, Int. J. Fract. ,180: 163-175, 2013.
[9] K. Uenishi, H. Yamachi, K. Yamagami, R. Sakamoto, Dynamic fragmentation of concrete using electric discharge impulses, *Constr. Build. Mater*. 67:170-179, 2014.